Drop-Landing Inverse Dynamics Model of Human Knee

Dumitru I. Caruntu[1]
Mechanical Engineering Department,
University of Texas Rio Grande Valley,
Edinburg, TX 78539
e-mails: dumitru.caruntu@utrgv.edu;
caruntud2@asme-member.org;
dcaruntu@yahoo.com

Ricardo Moreno
Mechanical Engineering Department,
University of Texas Rio Grande Valley,
Edinburg, TX 78539

This work investigates the kinematics and ligament, muscle, and contact forces of drop-landing exercise. A two-dimensional sagittal inverse dynamics knee model is developed to predict internal forces experienced during this exercise. Experimental data is gathered using a VICON motion analysis system and AMTI force plates. This experimental data is then used as input to the inverse dynamics model. The forces produced during the drop-landing exercise are computed using an optimization approach. The tibiofemoral contact point was predicted to move anteriorly as the most significant muscle, ligament, and contact forces increased reaching their peaks. Next, the contact point moves posteriorly as the most significant internal forces decrease, and then moves again anteriorly until the end of the exercise (end of the ascent phase) as the internal forces decrease to zero. Posterior cruciate ligament (PCL) is predicted to be the only significant ligament during drop-landing. The largest force values experienced during drop-landing are gluteus muscle and tibiofemoral contact forces with a peak of 17 body weight (BW), quadriceps muscle force with a peak of 14 BW, and hip contact force along femoral longitudinal direction with a peak of 7 BW. A comparison with data available in the literature is conducted. [DOI: 10.1115/1.4056356]

Keywords: inverse dynamics, human knee, drop-landing

1 Introduction

Landing mechanics is an essential part of airborne movements. Landing is considered to be natural as the human body seems to complete it subconsciously. Knee and ankle are the most injured joints and with the most severity, Dufek and Bates [1]. Ligament ruptures are terrible knee injuries that weaken athletic careers, Bates et al. [2]. About 75% of these injuries occur in dynamic situations, Norcross et al. [3]. In competitive athletics, landing is attributed to be the cause of anterior cruciate ligament (ACL) injuries, Pflum et al. [4]. About 200,000 ACL injuries transpire in the United States every year, Taylor et al. [5]. Dufek and Bates [1] identified that the landing phase is often inconsequential and effectively overlooked, which may prove unfavorable and result in injury.

These types of injuries can occur during a bipedal or one-legged landing sequence. One-legged landings are considerably more dangerous due to the fact there is a "decreased base of support and increased demand required by absorption of the impact of landing," Pappas et al. [6]. Laughlin et al. [7] mentioned that these occurrences correlate to "athletic maneuvers during significant and rapid decelerations of the body's center of mass." Some athletic maneuvers include cutting and rapid decelerations, landing from a jump knee hyperextension, and sudden deceleration with no change of direction, Earl et al. [8]. There is a general idea regarding the contributing factors that lead to these types of injuries. However, the mechanism of ACL injury is not entirely understood. Understanding landing mechanics would aid the development of injury-deterring methods, Afifi and Hinrichs [9].

Some landing mechanics that could be improved upon include joint kinematics and kinetics, landing style, muscle activation patterns, and energy absorption strategies, Pflum et al. [4]. Landing styles include toe-heel, flatfoot, toe-only, and heel-only, Dufek and Bates [1]. The main goal in landing is to dissipate or transfer the energy effectively that is produced by contact. Once making contact, then a series of movements are done by the joints and extensor muscle that contract eccentrically, doing negative work to absorb or dissipate energy, Prilutsky et al. [10].

Understanding these mechanisms, properly addressing the problems, and taking action could deter future complications. Investigating landing biomechanics is beneficial for performance-based tasks and injury prevention. Therefore, mathematical models are built for predicting the characteristics of the movement.

This work investigates the muscular, ligament, and contact forces that are associated with the drop-landing exercise, with a focus on contact forces and absorbing forces from impact due to landing. To predict internal forces that are experienced during landing, a two-dimensional knee model was built. The knee model uses an inverse dynamics approach in which the Newton-Euler dynamics equations of motion are equality constraints of the model. However, the difficulty lies in finding a "physiologically feasible set of controls" for the system, Schellenberg et al. [11]. In doing so, objective criterion and an objective could be defined on the motor task, Spägele et al. [12]. Partial results regarding the drop-landing exercise have been reported in the literature, especially in quantifying ACL strain, knee contact force, and vertical ground reaction force. To the best of our knowledge, this study expands on predicting ligament behavior, other than ACL, and on contact forces and tibiofemoral contact throughout the drop-landing exercise. Comparisons with other drop-landing exercises, and regular squat exercises, investigations reported in the literature are conducted.

2 Inverse Dynamics Anatomical Model of Human Leg

Musculoskeletal models are used to capture and provide objective criteria for various movements, Spägele et al. [12]. Present model focuses on the drop-landing exercise. Coordination, muscular strength, landing style, and anticipation are all factors important in landing. This study focuses on the lower limb, and implications that landing may have on the knee joint.

In this knee model is modeled as two rigid bodies, femur and tibia, that move relatively with respect to one another. A fixed *XY* global coordinate system is used to capture the entire movement of the exercise, and local coordinate systems with their origins at the centers of mass of femur and tibia are used to describe anatomical local geometry of the bones and ligament insertion points,

[1]Corresponding author.

Manuscript received January 3, 2022; final manuscript received November 14, 2022; published online December 19, 2022. Assoc. Editor: Lei Zuo.

Caruntu and Moreno [13]. Patellar flexion angle θ_{PF} is directly related to the tibiofemoral flexion angle θ_{TF} as follows $\theta_{PF} = 7\theta_{TF}/9$, Caruntu and Hefzy [14]. The patellofemoral contact force is to be predicted by the optimization used in inverse dynamics knee model. The angle of the patellar tendon α_{PT} with respect to the tibial shaft as a function of the tibiofemoral flexion angle used in this research is reported in the literature as $\alpha_{PT} = \pi/9 - 3\theta_{TF}/11$, De-Frate et al. [15].

2.1 Joint Articular Curves. The femoral articular joint curves are approximated by two circles [13]. The larger circle called patellofemoral circle approximates the femoral articular curve of the patellofemoral joint. The smaller circle, called tibiofemoral circle, approximates the femoral articular curve of the tibiofemoral joint. The patellofemoral circle is used for muscle insertions and patellofemoral contact. The work of Yue et al. [16] was used to calculate the length of the patellofemoral circle. They reported the anteroposterior length of the femoral condyle between two races and their genders. An assumption was made to acquire the anteroposterior length of femoral condyle of this study subject. The assumption is that the human bone structure is more related to a person's height than their race. The subject's height in this work was between the two races, and the calculated subject's anteroposterior length of the femoral condyle resulted about 7 cm, Yue et al. [16]. In this work subject is a male 1.75 m tall and 84 kg. When the knee undergoes flexion, tibia rotates about the posterior side of the femoral condyle. A tibiofemoral circle was introduced to fit the posterior side of the femoral condyle. The radius for the tibiofemoral circle was calculated using the work of Caruntu et al. [17], and Granados [18], where the X-ray was set to match the anteroposterior length of the subject's femoral condyle. Using MATLAB, the posterior geometry of the femoral condyle was traced to get the approximate radius for the tibiofemoral circle. The radius of the tibiofemoral circle resulted to be 2 cm. The tibiofemoral circle radius used was from Granados [18], and the location of the tibiofemoral circle center along the tibial plateau was calculated using Hill et al. [19]. At 90 deg tibiofemoral flexion angle, the posterior center measured 2 cm anterior from the posterior edge of the tibial plateau, Hill et al. [19]. So, the center was placed 2 cm parallel to the tibial plateau, plus the tibiofemoral radius perpendicular to the tibial plateau at 90 deg knee flexion. The tibiofemoral circle center has a motion parallel to the tibial plateau during the exercise [13].

2.2 Muscle, Ligament, and Contact Forces. Muscles and muscle forces included in present model are given in Table 1. Hamstrings F_h and quadriceps F_q muscle forces are given by

$$F_h = F_{\text{fbl}} + F_{\text{bfs}}, \quad F_q = F_{rf} + F_v \tag{1}$$

Some assumptions for muscles are as follows. Gastrocnemius muscle is parallel to the tibial longitudinal axis, the orientation used for the patellar tendon is given by De-Frate et al. [15], and the magnitude of patellar tendon force is same as the quadriceps force. For femur, the hamstrings force is assumed to be parallel to the femoral longitudinal axis, and the direction of the gluteus and iliacus are assumed to be 45 deg with respect to the femoral longitudinal axis.

Table 1 Muscle forces in the model

Force	Muscle
F_{bfl}	Biceps femoris long head
F_{bfs}	Biceps femoris short head
F_{rf}	Rectus femoris
F_{gas}	Gastrocnemius
F_g	Gluteus
F_i	Iliacus
F_v	Vasti
F_h	Hamstrings
F_q	Quadriceps

Table 2 Ligament forces in the model

Force	Ligament
F_{acl}	Anterior cruciate ligament (ACL)
F_{pcl}	Posterior cruciate ligament (PCL)
F_{lcl}	Lateral collateral ligament (LCL)
F_{mcl}	Medial collateral ligament (MCL)

Four major ligaments hold the knee joint together limiting the relative motion between femur and tibia. The ligaments included in the model and their forces are given in Table 2. Both ligament insertion points and tibiofemoral contact points are related to the tibiofemoral center of rotation, so it was imperative to find such a suitable point. A virtual marker was added adjusting the proper location of the tibiofemoral center of rotation, Caruntu and Moreno [13], without altering any other point in the model. Ligaments' insertion points were then placed for standing position, Shelburne and Pandy [20]. The insertion points were then related to their respective body, i.e., femoral insertion with the tibiofemoral center and the tibial insertion with respect to the tibial plateau. The ligaments have a nonlinear string-like behavior, only providing force under strain. The nonlinear ligament force F_ℓ expression used for ACL, lateral collateral ligament (LCL), and medial collateral ligament (MCL) is given by [14]

$$F_\ell = \begin{cases} 0 & \epsilon \le 0 \\ k_q(L - L_0)^2 & 0 \le \epsilon \le 2\epsilon_0 \\ k_\ell[L - (1 + \epsilon_0)L_0] & 2\epsilon_0 \le \epsilon \end{cases} \tag{2}$$

where ϵ, k_q, k_ℓ, L, and L_0 are the strain, stiffness coefficient of quadratic region, stiffness coefficient of linear region, current length, and slack length of the ligament, respectively. The linear range threshold was specified as $\epsilon_0 = 0.03$, [14]. The coordinates of the ligamentous insertion points, slack lengths, and stiffness coefficients used were reported in the literature [21].

There were some complications with modeling PCL in this fashion. The medial and lateral markers were placed on the most prominent part of the knee, which is denoted as the transepicondyler axis, Most et al. [22]. The knee model captured the motion of the transepicondylar axis but not the geometric center axis, which depicts the true motion of the knee. Since the geometric center axis has an unusual behavior under flexion, described by Most et al. [22], the PCL was the only ligament largely affected by this ineffective description. For this present knee model, the PCL was left to be optimized but the insertions were anatomically based. Ligaments must be in tension to produce forces.

Contact forces of tibiofemoral, patellofemoral, and hip joints are included in the model. They have five components as follows: two components of the tibiofemoral contact force, two components of the hip contact force, and the patellofemoral contact force, given in Table 3. The component F_{cx} is assumed to be zero

Table 3 Contact forces in the model

Force	Contact forces
F_{cx}	Tibiofemoral contact force parallel to the tibial plateau (due to friction)
F_{cy}	Tibiofemoral contact force perpendicular to the tibial plateau
F_{hx}	Hip contact force perpendicular to femoral longitudinal direction
F_{hy}	Hip contact force parallel to femoral longitudinal direction
F_{cp}	Patellofemoral contact force

due to the lack of contact friction in the tibiofemoral joint. Contact forces are not zero if there is contact between bones. Although patella is not included in the investigation, the direction of the patellofemoral contact force is captured and modeled as a force on the femoral condyle, and its magnitude is determined through the optimization process of the inverse dynamics model.

2.3 Inverse Dynamics Model. An inverse dynamic approach is used in this work. Subject's femoral and tibial segment lengths, their radii of gyration, mass, centers of mass, and moments of inertia were determined using Winter [23]. The exercise was captured using an integrated system consisting of a VICON Motion Analysis System and AMTI Force Plates housed in the Biomechanics Laboratory, Director Caruntu, at the University of Texas Rio Grande Valley. The experimental data was used to determine the six accelerations of the system consisting of the sagittal plane accelerations of the centers of mass of femur and tibia and their body angular accelerations. These accelerations, femoral and tibial masses, and moments of inertia, as well as the ground reaction forces that are experimentally determined, were used as input data to the six Newton-Euler differential equations describing the sagittal plane motions of femur and tibia. Newton equations are written in X and Y directions, and Euler equations are in the Z direction for each body. Figures 1 and 2 show the free-body diagrams of femur and tibia [13].

The unknowns of the system are muscle, ligament and contact forces, and tibiofemoral contact location. The number of unknowns of the system is 19, as follows: four ligament forces, five contact forces, nine muscle forces, and the location of the tibiofemoral contact point, Tables 1–3. The number of equations describing the system is 12 as follows: six Newton-Euler equations of motion, and another six equations that use experimental data to calculate ligament forces, state no joint friction assumption, and calculate hamstrings and quadriceps forces from component muscle forces. The last six equations are as follows. Three equations are used to calculate directly from the experimental data the three ligament forces F_{acl}, F_{lcl}, and F_{mcl}, see Eq. (2), another equation for the assumption of no friction in the knee joint is $F_{\text{cx}} = 0$, and two more equations, see Eq. (1), are used to calculate forces in hamstrings and quadriceps muscles, F_h and F_q, respectively, from muscle forces predicted by optimization.

Therefore, the system to be solved consists of six Newton-Euler dynamics equations and 13 unknowns. Such system is undetermined having an infinite number of possible solutions. However, if the system is subjected to an optimization with feasible constrains, only one of the results is the optimal solution of the system. In this work, the optimal solution is considered when the body uses the least amount of force to reproduce the motion.

The optimization problem to be solved is as follows. The unknowns of the optimization problem are 13 as follows: ligament force F_{pcl}, four contact forces F_{cy}, F_{hx}, F_{hy}, F_{cp}, seven muscle forces F_{bfl}, F_{rf}, F_g, F_i, F_v, F_{bfs}, F_{gas}, and the location of the tibiofemoral contact point denoted by D which is the distance between the contact point and the most posterior point of the tibial plateau. The objective function f to be minimized is the sum of squares of forces in muscles, PCL, and contact forces

$$\min f = F_{\text{bfl}}^2 + F_{\text{bfs}}^2 + F_{\text{rf}}^2 + F_v^2 + F_g^2 + F_i^2 + F_{\text{gas}}^2 + F_{\text{pcl}}^2 + F_{\text{cp}}^2 + F_{\text{cy}}^2 + F_{\text{hx}}^2 + F_{\text{hy}}^2 \tag{3}$$

with the unknowns satisfying 13 inequality constraints

$$F_{\text{bfl}} \geq 0, F_{\text{rf}} \geq 0, F_{\text{cy}} \geq 0, F_g \geq 0, F_i \geq 0, F_{\text{hx}} \geq 0, F_{\text{hy}} \geq 0 \\ F_v \geq 0, F_{\text{bfs}} \geq 0, F_{\text{gas}} \geq 0, F_{\text{cp}} \geq 0, F_{\text{pcl}} \geq 0, D \geq 0 \tag{4}$$

and six equality constraints given by the equations of motion in the sagittal plane using Newton's 2nd Law on the X and Y directions, and Euler equation on the Z direction for each body

$$\sum F_{Xi} = m_i \times a_{XCi}, \sum F_{Yi} = m_i \times a_{YCi}, \sum M_{Ci} = I_{Ci} \times \alpha_i \tag{5}$$

where subscripts are $i = 1$ for tibia, $i = 2$ for femur, C for center of mass; F_{Xi}, F_{Yi}, M_{Ci}, I_{Ci} are forces, moments, and moments of inertia, respectively; a_{XCi}, a_{YCi}, α_i are linear accelerations of C,

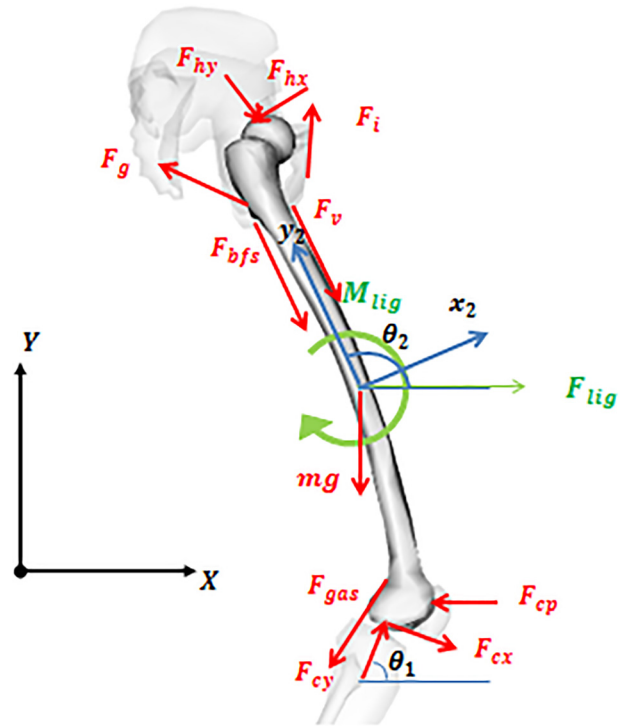

Fig. 1 Free body diagram of femur [13]

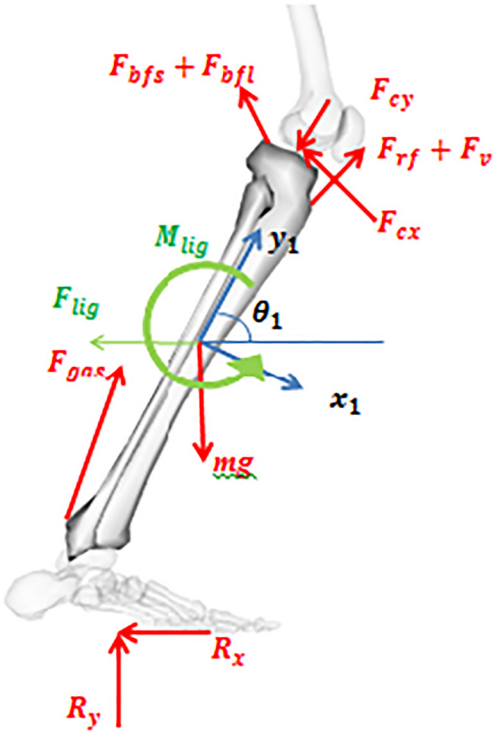

Fig. 2 Free body diagram of tibia [13]

and angular accelerations of the corresponding bodies, respectively, [13].

The quantitative calculation of muscle forces and internal loads is the overall objective of this study, Blajer et al. [24].

In conclusion, the inverse dynamics knee model consists of minimizing the objective function above subject to six equality constraints (six Newton-Euler equations) and 13 inequality constraints stating that muscle, ligament, and contact forces, as well as the distance between the tibiofemoral contact point and the posterior edge of tibial plateau, must be positive. These conditions are necessary since muscles and ligaments must be in tension to produce forces, the bones must be in contact to produce contact forces, and the tibiofemoral contact point must be on the tibial plateau.

3 Drop-Landing Exercise and Experimental Work

The drop landing trial starts on top of a platform, standing upright at the edge of the platform. The platform has a height of 38 cm and it was placed 15 cm away from the force plates, similar to Laughlin et al. [7], Fig. 3. Niu et al. [25] provided a range of platforms used for other studies, and for the this work the platform height was within this range of 10–60 cm. The arms were to be kept akimbo, i.e., placed on the hips and elbows tuned outward. The subject pushes off from one foot and aims to land in the center of the force plates. Once pushing off, the subject lands on one foot (one-legged landing).

The subject was 1.75 m tall and had a mass of 84 kg. Reflective markers were placed on the subject marking key anatomical points, Fig. 3, locations are as follows: the furthest point on the toe, heel, lateral and medial ankle, lateral and medial knee, shin, hip, and the front and rear of the torso. Shells were placed on the foot, shank, and thigh, and are a vital part of the tracking process. Shells were used when the captured data experienced a "gap," or occurrences where the marker was not captured. This may be due to marker being covered or the marker not reflecting enough. Shells aided the program to calculate the position of the marker whenever a gap occurred. This captured data was used for the knee model.

The instrumentation used to collect the experimental data consisted of synchronized two 60 cm × 60 cm AMTI force plates collecting data at a sampling rate of 1000 Hz and ten VICON MX T-Series infrared cameras recording the coordinates of each marker at a sampling rate of 100 Hz. The two AMTI force plates provided ground reaction forces in *x*-, *y*-, and *z*- directions, moments about the *x*-, *y*-, and *z*-directions, and centers of pressure about the *x*- and *y*- directions. This data was used as input data for the inverse dynamics model. The ten VICON cameras captured the light reflected from the markers as the subject performed the task. The cameras recorded the trajectories of all markers. The cameras face toward a closed area to fully view the task and minimize experimental error.

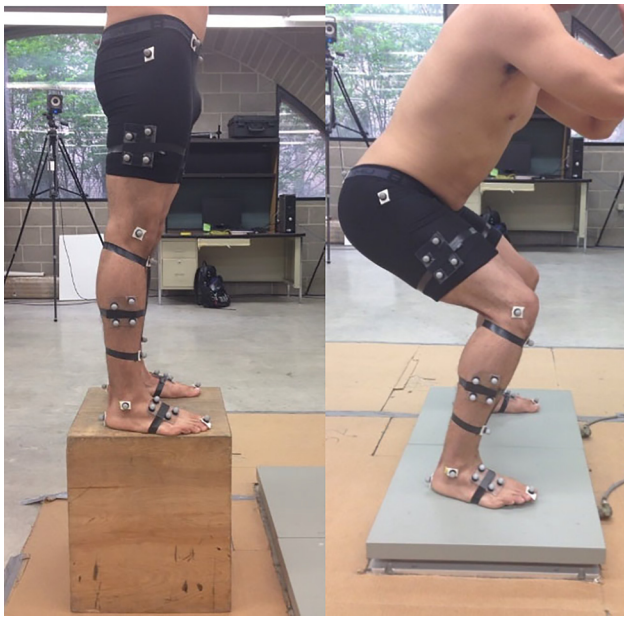

Fig. 3 Starting and landing positions of the drop-landing exercise

The protocol followed for the drop-landing exercise is as follows. The subject was required to perform warm-up exercises and dynamic stretching before conducting the test. The warm-up exercise consisted of walking lunges, high knees, and practicing landing squats. Once completing the five-minute warm-up routine, the subject was then instructed to complete drop-landing protocol. The test is comprised of five drops from a platform, which is a test based on contact and energy dissipation. Landing is the main objective of this study, and the subject must adhere to the "soft" landing guidelines. Following a toe-heel technique, as described by Dufek and Bates [1], and squatting down upon impact to dampen the force ensures a soft landing. Then, the subject will return to the standing position, indicating the end of the experiment. The depth of the dampening squat is determined similarly to Samozino et al. [26], where the subject must attempt to have a 90 deg knee flexion angle while maintaining balance. If the subject does not get the proper squat angle, if there's an imbalance, or if any inefficient landing technique is either visible or announced by the subject, the trial is discarded and replaced by a complete trial after the proper rest period. After every test, completed or failed the subject must wait two minutes before attempting another trial. This was done to avoid any fatigue that might be encountered.

The experimental data was filtered. The experiments were captured and processed by the VICON Nexus software. Collected data was then exported onto an excel spreadsheet where the marker and force plate data was compiled. "The collected data (raw data) were filtered using a low-pass, fourth-order, zero-lag Butterworth filter with a cutoff frequency of 30 Hz resulting from the residual analysis of the experimental data," [13]. This data served as input data for the two-dimensional (sagittal) human leg anatomical model.

The velocities and accelerations were calculated using numerical differentiation as follows

$$v_{i+1/2} = (s_{i+1} - s_i)/\Delta t, \quad a_{i+1} = (v_{i+3/2} - v_{i+1/2})/\Delta t \qquad (6)$$

respectively, where s is the position data, v is the velocity, a is the acceleration, and Δt is the time interval between two consecutive frames. One can notice that the velocities were calculated halfway between sample times [13]. The angular velocities and angular accelerations were computed in a similar fashion. Since the frame rate is 100 Hz, $\Delta t = 0.01$ s. Both linear and angular velocities and accelerations were also filtered. These calculations were then used for the Newton-Euler equations of motion for the two-dimensional model.

4 Numerical Simulations

The main focus of this investigation of the drop-landing exercise consists of internal forces produced and tibiofemoral contact point travel during the exercise. The standing positions and airborne positions are ignored. Time zero is when the subject makes contact with the force plates. The vertical line of about 0.3 s in Fig. 4 is the instant when the subject is at deepest part of the squat. A description of this progression is shown on top of Fig. 4.

Figure 4 illustrates the tibiofemoral flexion angle. In this exercise, the subject reached about 100 deg flexion angle in an effort of dissipating the landing energy.

Figure 5(*a*) shows the experimentally measured ground reaction forces (GRFs) to the drop-landing exercise. From this graph, a

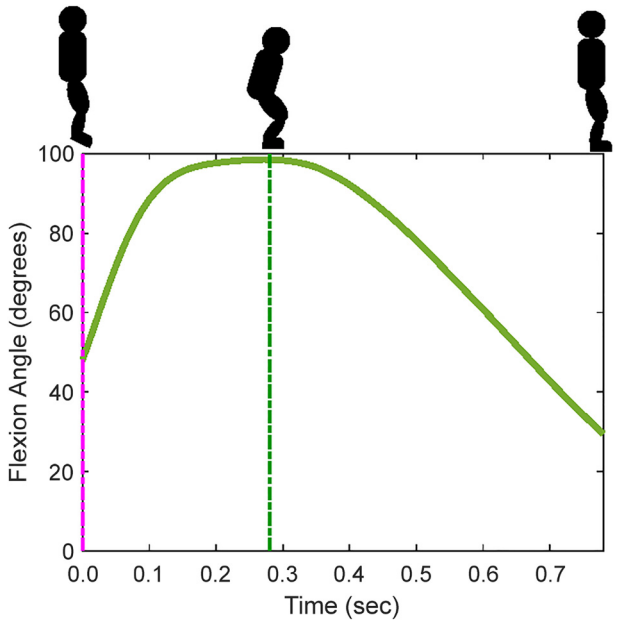

Fig. 4 Flexion angle for the drop-landing exercise

bimodal force-time curve of the vertical GRF component R_y can be seen, so a toe-heel landing style could be inferred, Dufek and Bates [1]. The maximum R_y value was about 4 BW. The subject used the dampening squat to dissipate the landing energy. One can notice that landing energy was dissipated in about 0.3 s. However, it took about 0.7 s to return back to normal, same time as performing the entire dampening squat exercise.

Figures 5(*b*)–5(*f*) show the model prediction of muscle, contact, and ligament forces, as well as the travel of the tibio-femoral contact point for the exercise.

Figure 5(*b*) illustrates the muscle force production, F_q quadriceps force, F_h hamstrings force, and F_{qas} gastrocnemius force, during the drop-landing exercise. The quadriceps muscle F_q produces the most amount of force. The model predicts that the quadriceps force F_q has a peak of about 14 BW, about 11.5 kN for this work subject, in the first 0.2 s of landing, and maintains values between 10.5 BW and 10 BW for another 0.1 s until the subject reaches the de-epest squat posture of the exercise. Therefore, the landing energy is dissipated in the first 0.3 s of the exercise. From 0.3 s to 0.8 s the quadriceps force decreases to 1 BW as the subject completes the ascent phase of the squat exercise.

Figure 5(*c*) shows knee and the hip contact forces during the exercise. The normal contact force in the knee F_{cy}, i.e., the force perpendicular to the tibial plateau, is the force that experiences the largest values reaching a peak of 17 BW. The hip force component that is parallel to the longitudinal axis of the femur F_{hy} is the second force experiencing large values, reaching a peak of about 7.5 BW. The other hip force component that is perpendicular to the longitudinal axis of the femur F_{hx} experiences its maximum of about 1 BW at the de-epest flexion angle in the squat. The patellofemoral contact force F_{cp} reaches a maximum of about 6 BW. All contact forces, except F_{hx}, experience their highest peak 0.1 s after impact, and they significantly decrease from 0.2 s to 0.7 s.

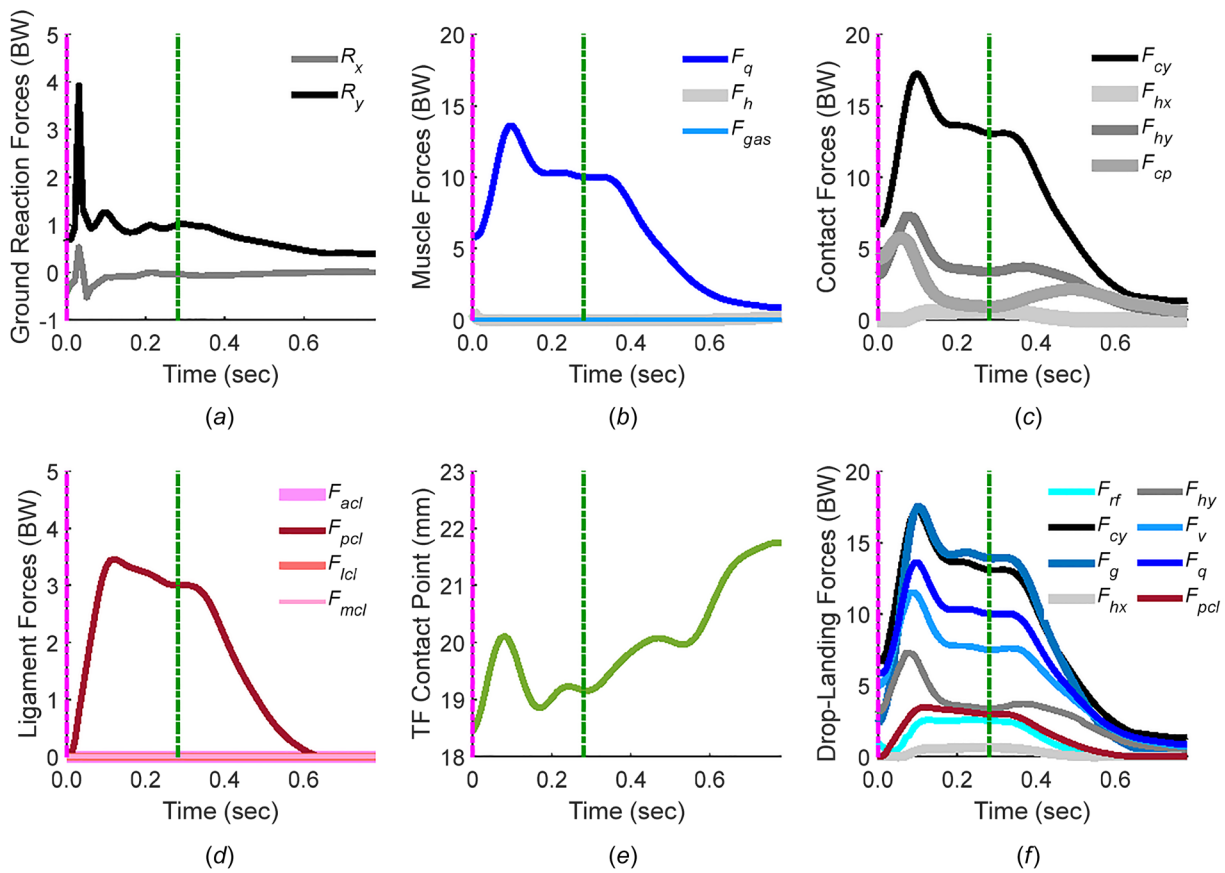

Fig. 5 Drop-landing exercise: (*a*) ground reaction forces R_x horizontal anterior component, and R_y vertical upward component; (*b*) muscle forces F_q quadriceps force, F_h hamstrings force, and F_{gas} gastrocnemius force; (*c*) Contact forces F_{cy} tibiofemoral normal contact force, F_{cp} patellofemoral contact force, F_{hx} and F_{hy} hip contact forces; (*d*) ligament forces during the drop-landing exercise, F_{pcl} posterior cruciate ligament, F_{acl} anterior cruciate ligament, F_{lcl} lateral colateral ligament, and F_{mcl} medial colateral ligament; (*e*) distance between the tibiofemoral contact point and the posterior edge of the tibial plateau; and (*f*) significant forces during the exercise

Figure 5(*d*) shows that the posterior cruciate ligament (PCL) is the main contributor of the drop-landing exercise. PCL force reaches its peak of about 3.5 BW (or about 2.9 kN) around 0.1 s and maintains values above 3 BW for the descent phase of the squatting, i.e., until about 0.3 s. Cleather et al. [27] reported that the failure limit for the PCL in healthy males is about 4.5 kN. The PCL force then decreases and reaches zero during the ascent phase.

Figure 5(*e*) illustrates the distance in mm between the tibiofemoral contact point and the posterior edge of the tibial plateau. The contact point moves anteriorly about 1.5 mm in the first 0.1 s, which is the time when muscle and contact forces reach their peaks. Between 0.1 s and 0.2 s, as the muscle and contact forces decrease, the contact point moves 1.3 mm posteriorly. As the descent phase of squatting continues the contact point moves anteriorly about 0.5 mm. During the ascent phase of the squat between about 0.3 s and 0.8 s the contact point continues to move anteriorly another 2.6 mm.

Figure 5(*f*) displays the significant forces during the drop-landing exercise. Forces not represented in this figure were negligible, except F_{cp} that can be seen in Fig. 3(*c*). The largest forces that were experienced were the tibiofemoral contact force F_{cy}, quadriceps force F_q, hip contact force F_{hy}, and gluteus muscle force F_g. This figure gives a better comprehension of the forces that are experienced during landing.

5 Discussion

Figures 6(*a*)–6(*c*) compare the results of this work with other investigations on drop-landing exercises reported in the literature, and Figs. 6(*d*)–6(*f*) with investigations on regular squat exercise. Every investigation has a different execution time for exercise. However, the time of interest in drop-landing exercise is the time of impact. Therefore, all the data is shifted to measure from the instant of impact (t = 0 s) to about 0.3 s, the time frame where the landing energy is dissipated.

Figure 6(*a*) shows a comparison of GRFs of drop-landing exercise of this work and data available in the literature. If the movement was performed in a similar fashion to the other studies, then the GRFs in the this study should be like the ones reported in the literature. In Fig. 6(*a*), the prediction of 4 BW peak of GRF and the overall behavior are in agreement with Laughlin et al. [7] (peak of 3.5 BW). Pflum et al. [4] reported a similar GRF behavior, with a peak magnitude of 3 BW. This work and the two mentioned references show that the magnitude of GRFs reduces to 1–1.5 BW after 0.1 s.

Figure 6(*b*) shows a comparison of the drop-landing tibiofemoral contact force between this work and Kernozek et al. [28]. Both studies display a similar behavior, the contact force increases until reaches a peak and then decreases continuously. There is an agreement that there is a peak of the contact force, and this peak occurs within the first 0.2 s of landing, more specifically it occurs at 0.1 s. This is the same time interval of 0.2 s for which most of the forces experience their peak values. There is a difference in magnitude between the two data. The peak contact force for this study is 17 BW, while Kernozek et al. [28] reported a value of 8 BW. This work deals with one-legged landing exercise while Kernozek et al. [28] with two-legged landing exercise.

Figure 6(*c*) illustrates a comparison of drop-landing vasti muscle forces between this work and Pflum et al. [4]. They reported data for vasti muscles since they were the muscles that experienced the largest forces. The data predictions in this are in

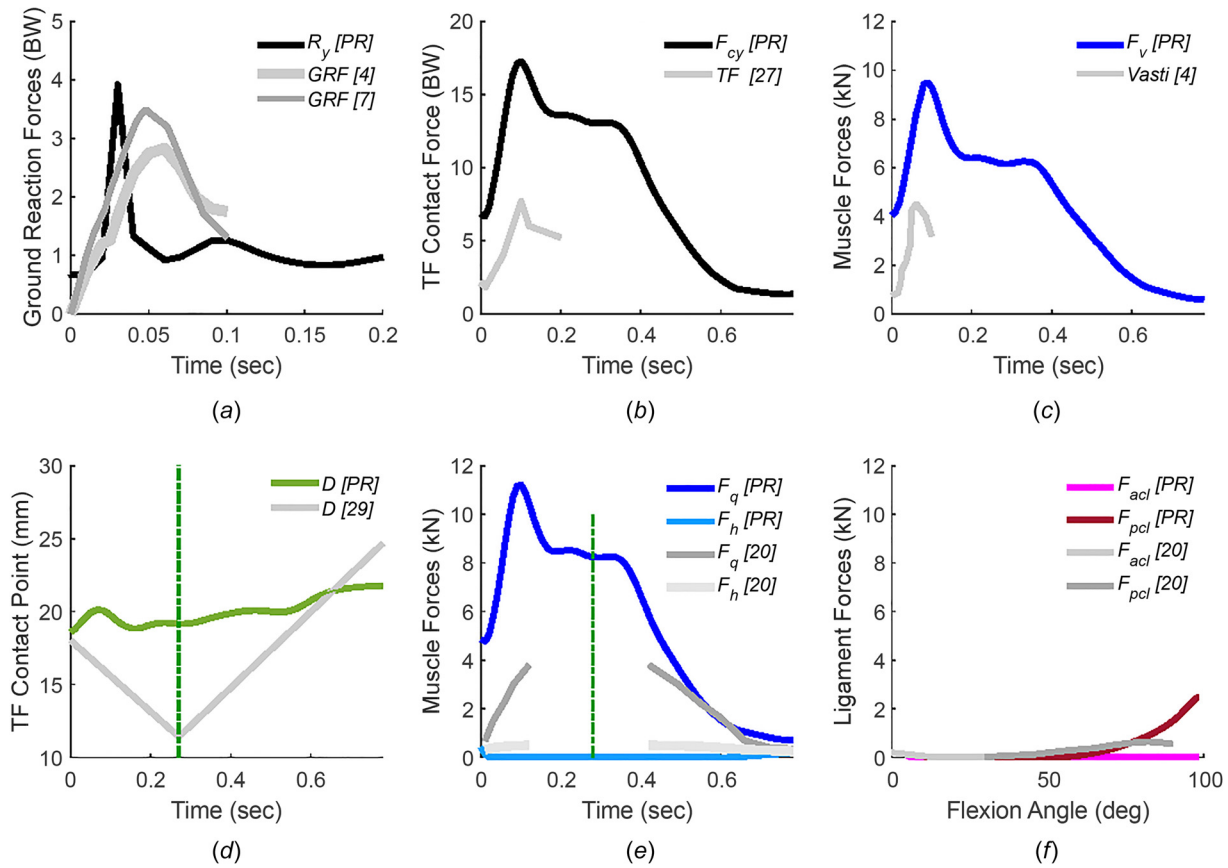

Fig. 6 Comparison drop-landing versus drop-landing: (*a*) vertical ground reaction force comparison: this work [PR] versus Pflum et al. [4] and Laughlin et al. [7]; (*b*) tibiofemoral contact force: this work versus Kernozek et al. [28]; (*c*) vasti muscle force: this work versus Pflum et al. [4]; comparison drop-landing versus regular Squat: (*d*) distance between the tibiofemoral contact point and the posterior edge of the tibial plateau: this work versus Murakami et al. [29]; (*e*) Quadriceps and hamstrings muscle forces this work versus Shelburne and Pandy [20]; and (*f*) Cruciate ligament forces: this work versus Shelburne and Pandy [20]

agreement with Ref. [4] showing the same behavior. The peak values are experienced in a 0.2 s time frame.

Figure 6(*d*) illustrates a comparison between the contact point behavior during drop-landing (this work) and regular squat exercise [29], since drop-landing exercise is in fact a landing squat exercise. One can notice that the contact point during drop-landing remains within the travel range of the regular squat exercise contact point. Moreover, the contact point during drop-landing has a much smaller range of motion. The ascent phase from about 0.3 s to 0.8 s shows a motion in the anterior direction of the contact point for both exercises, drop-landing, and regular squat exercise. However, during the rapid breaking descent phase of drop-landing there is an anterior shift that is caused by the impact. This is opposite to the motion of the contact point in the posterior direction during regular squat exercise.

Figure 6(*e*) shows the quadriceps and hamstrings muscle forces from the drop-landing exercise (this work) compared to regular squat data [20]. The vertical line in Fig. 6(*e*) represents the instance where the subject achieves the largest flexion angle. The first part of the landing is the descent phase where the subject goes from 50 deg to 100 deg of flexion angle. Then, the second part is the ascent phase where the subject goes from 100 deg of flexion angle to standing, Fig. 4. There is an agreement between this work and Shelburne and Pandy [20] in terms of the behavior of the quadriceps and hamstrings muscle forces during squat phases. However, there are differences in terms of magnitudes. The ascent phase of the squat in the drop-landing exercise agrees better in the latter half of the exercise. Differences in magnitudes during the descent phase were expected since in drop-landing, the subject experiences from the beginning of landing much larger forces than the regular squat exercise.

Figure 6(*f*) compares ligament forces during drop-landing (this work) and regular squat exercise [20]. The predicted results of this work are in agreement with data reported by Shelburne and Pandy [20]: (1) ACL force is less than 200 N and decreases with flexion angle for flexion angles less than 10 deg and it is zero for flexion angles greater than 10 deg, (2) PCL force is zero for flexion angles less than 30 deg (squat exercise) and 50 deg (drop-landing) and then increases with flexion angle. Also, (3) PCL force reaches values between 600 and 700 N around 80 deg of flexion for both exercises. Significant differences are in deep squatting, where the PCL force remains around 550 N between 80 deg and 90 deg flexion angle for the squat exercise, while for drop-landing reaches 2500 N around 100 deg flexion angle. The squat in the drop-landing exercise has to dissipate the landing energy.

6 Conclusions

This work expands on data available for the drop-landing exercise. The exercise consisted of two phases. The first phase of about 0.3 s was the descent landing squat, and the second phase of about 0.5 s was the ascent squat. New predictions regarding the contact point, knee ligaments, and hip joint forces are reported. The contact point was predicted to (1) move 1.5 mm anteriorly for 0.1 s just like the most significant muscle, ligament, and contact forces, Fig. 5(*f*), increased reaching their peaks, (2) next move 1.3 mm posteriorly until 0.2 s as the most significant internal forces decreased to some extent, and (3) then move 0.4 mm anteriorly until about 0.3 s, i.e., the end of the descent phase of the landing squat, as the most significant internal forces experience approximately a plateau. For the ascent phase, between 0.3 s and 0.8 s, the contact point movers anteriorly 2.6 mm. PCL ligament is predicted to be the only significant ligament during drop-landing. It reaches a peak of 3.5 BW after 0.1 s and then decreases to zero throughout the rest of the descent phase and the ascent phase.

The largest muscle and contact forces experienced during drop-landing were gluteus and tibiofemoral normal contact forces, both reaching a peak of 17 BW, quadriceps force reaching a peak of 14 BW, vasti muscles with a peak of 12 BW showing that is the most important component of the quadriceps force, and the hip contact force F_{hy} with a peak of 7 BW. Therefore, the hip contact forces are predicted to be significant with a lesser magnitude than knee contact forces.

In drop-landing exercise, mitigating the contact forces is the overall goal for any landing-based exercises. There is only a short period of time in which the body could absorb or dissipate the energy, which could explain the large magnitudes of force. When dropping from a platform there is no change in direction like in a regular jump exercise, in which muscles are already activated to jump. This may lead to a disadvantage in landing due to a loss of sensation.

Differences between studies occurred, but the overall trend was similar. Different studies have different sets of protocols and procedures. One can mention different drop heights, different distances, and landing styles. Standardizing the protocol may improve the comparability of studies and validate any future work in this exercise. Figures 6(*b*), 6(*c*), and 6(*e*) show some differences between this work and data reported in the literature. Table 4 summarizes the drop heights, landing styles, and subject's weight of this work and Refs. [4,7,28]. In this work and Refs. [4,7] the subject steps off from a platform of 38 cm, 60 cm, and 37 cm, respectively, while in Ref. [28] the subject drops off from a 60 cm hang bar. In terms of landing, this work and Ref. [7] investigated one-legged landing, while Refs. [4,28] investigated two-legged landing. This work and Ref. [4], and Refs. [7] and [28], have similar subject's weights. Table 4 also summarizes the peaks of GRF, tibiofemoral contact force, and vasti muscle force. This work of one-legged landing exercise with a peak of 4 BW of the ground rection forces is in agreement the one-legged landing exercise of Ref. [7] that reported 3.5 BW. This work is also in agreement with the fact that one-legged landing exercises show a larger GRF peak than two-legged landing exercises [4,28]. The difference in terms of tibiofemoral contact force peak between 17 BW and 8 BW of this work and Ref. [28], respectively, is explained by the fact that in this work the exercise is one-legged landing while in Ref. [28] the exercise is two-legged landing. The difference between 9.5 kN and 4.5 kN Vasti muscle force peaks between this work and Ref. [4], respectively, is due to the fact that in this work the exercise is one-legged landing while in Ref. [4] the exercise is two-legged landing.

Figures 6(*d*), 6(*e*), and 6(*f*) show a comparison between the drop-landing exercise of this work and regular squat exercise reported in the literature [20,29]. Table 5 summarizes the comparison. One can notice in Fig. 6(*d*) that for the regular squat exercise, the tibiofemoral contact point travels 5.5 mm posteriorly during the descent phase, and about 14 mm anteriorly during the ascent phase [29], while this work predicts that the tibiofemoral contact point has a much lesser travel due to the large muscle and

Table 4 Comparison drop-landing versus drop-landing (Figs. 6(*a*), 6(*b*), and 6(*c*))

Reference	Drop	Landing	Subject's weight	GRF peak	TF contact force peak	Vasti muscle force peak
This work	Step off from 38 cm platform	One-legged	84.0 kg	4.0 BW	17 BW	9.5 kN
Laughlin et al. [7]	Step off from 37 cm platform	One-legged	63.2 kg	3.5 BW		
Pflum et al. [4]	Step off from 60 cm platform	Two-legged	82.0 kg	2.8 BW		4.5 kN
Kernozek et al. [28]	Drop off from 60 cm hang bar	Two-legged	62.6 kg	1.8 BW	8 BW	

Table 5 Comparison drop-landing versus regular squat (Figs. 6(*d*), 6(*e*), and 6(*f*))

Reference	Exercise	TF contact point. Peak travel during landing and descent phase	TF contact point. Peak travel during ascent phase	Quadriceps force Fq peak	Hamstrings force Fh	Posterior cruciate ligament force, Fpcl at 90 deg knee flexion
This work	Drop-Landing. Step off from 38 cm platform. One-legged landing	1.5 mm anteriorly, next 1.3 mm posteriorly, and then 0.4 mm anteriorly	2.6 mm anteriorly	11.2 kN	0.1 kN	1.7 kN
Mukarami et al. [29]	Two-legged squat exercise	5.5 mm posteriorly	14 mm anteriorly			
Shelburne and Pandy [20]	Two-legged squat exercise. Statics.			3.8 kN	0.2 kN	0.7 kN

ligament forces of the drop-landing exercise. The peak of the quadriceps force is about three times larger for the drop-landing than for regular squat exercise, Fig. 6(*e*), and the ACL force at 90 deg knee flexion is more than twice larger for the drop-landing than squat exercise, Fig. 6(*f*).

In conclusion, this work highlights the importance that landing plays in energy dissipation during impact.

Present model has limitations. First, the input data for the knee model was derived from only one set of data from one subject for the drop-landing exercise. Second, this model is a simplified representation of the knee joint, where the femoral condyle is modeled by two circles and the tibial plateau as a straight line. Third, this is two-dimensional model, so any internal-external rotation is neglected and the medial and lateral contact forces in the knee are not differentiated. Fourth, the tibiofemoral center of rotation motion is not entirely captured. The marker-based approach captures the transepicondylar axis motion described by Most et al. [22], but the geometric center axis is the correct axis for the tibiofemoral center of rotation. The ligament insertion points and contact points were related to this point, so there may be some improvements in the ligament and contact behavior. Fifth, the patellofemoral contact force is calculated from the optimization and is directly related to the quadriceps and patellar tendon forces.

More could be done with the drop-landing exercise. Effects of landing styles, drop heights, and other factors could be investigated in the protocol. Applying the geometric center axis would better describe the motion of the femoral condyle and the ligament behavior. Adding articular cartilage for deformable contact would also make the model more anatomical. Defining anatomically correct geometry would make the model more refined and would replicate more accurately.

Funding Data

- National Science Foundation CBET Division (Grant No. #1126763; Funder ID: 10.13039/100000001).

Data Availability Statement

The authors attest that all data for this study are included in the paper.

References

[1] Dufek, J. S., and Bates, B. T., 1991, "Biomechanical Factors Associated With Injury During Landing in Jump Sports," Sports Med., **12**(5), pp. 326–337.

[2] Bates, N. A., Ford, K. R., Myer, G. D., and Hewett, T. E., 2013, "Impact Differences in Ground Reaction Force and Center of Mass Between the First and Second Landing Phases of a Drop Vertical Jump and Their Implications for Injury Risk Assessment," J. Biomech., **46**(7), pp. 1237–1241.

[3] Norcross, M. F., Lewek, M. D., Padua, D. A., Shultz, S. J., Weinhold, P. S., and Blackburn, J. T., 2013, "Lower Extremity Energy Absorption and Biomechanics During Landing, Part I: Sagittal-Plane Energy Absorption Analyses," J. Athl. Train., **48**(6), pp. 748–756.

[4] Pflum, M. A., Shelburne, K. B., Torry, M. R., Decker, M. J., and Pandy, M. G., 2004, "Model Prediction of Anterior Cruciate Ligament Force During Drop-Landings," Med. Sci. Sports Exerc., **36**(11), pp. 1949–1958.

[5] Taylor, K. A., Terry, M. E., Utturkar, G. M., Spritzer, C. E., Queen, R. M., Irribarra, L. A., Garrett, W. E., and DeFrate, L. E., 2011, "Measurement of In Vivo Anterior Cruciate Ligament Strain During Dynamic Jump Landing," J. Biomech., **44**(3), pp. 365–371.

[6] Pappas, E., Hagins, M., Sheikhzadeh, A., Nordin, M., and Rose, D., 2007, "Biomechanical Differences Between Unilateral and Bilateral Landings From a Jump: Gender Differences," Clin. J. Sport Med., **17**(4), pp. 263–268.

[7] Laughlin, W. A., Weinhandl, J. T., Kernozek, T. W., Cobb, S. C., Keenan, K. G., and O'Connor, K. M., 2011, "The Effects of Single-Leg Landing Technique on ACL Loading," J. Biomech., **44**(10), pp. 1845–1851.

[8] Earl, J. E., Monteiro, S. K., and Snyde, K. R., 2007, "Differences in Lower Extremity Kinematics Between a Bilateral Drop-Vertical Jump and a Single-Leg Step-Down," J. Orthop. Sports Phys. Ther., **37**(5), pp. 245–252.

[9] Afifi, M., and Hinrichs, R. N., 2012, "A Mechanics Comparison Between Landing From a Countermovement Jump and Landing From Stepping Off a Box," J. Appl. Biomech., **28**(1), pp. 1–9.

[10] Prilutsky, B. I., and Zatsiorsky, V. M., 1994, "Tendon Action of Two-Joint Muscles: Transfer of Mechanical Energy Between Joints During Jumping, Landing, and Running," J. Biomech., **27**(1), pp. 25–34.

[11] Schellenberg, F., Oberhofer, K., Taylor, W. R., Lorenzetti, S., and Sun, Z., 2015, "Review of Modelling Techniques for In Vivo Muscle Force Estimation in the Lower Extremities During Strength Training," Comput. Math. Methods Med., **2015**(1), pp. 1–12.

[12] Spägele, T., Kistner, A., and Gollhofer, A., 1999, "A Multi-Phase Optimal Control Technique for the Simulation of a Human Vertical Jump," J. Biomech., **32**(1), pp. 87–91.

[13] Caruntu, D. I., and Moreno, R., 2019, "Human Knee Inverse Dynamics Model of Vertical Jump Exercise," ASME J. Comput. Nonlinear Dyn., **14**(10), p. 101005.

[14] Caruntu, D. I., and Hefzy, M. S., 2004, "3-D Anatomically Based Dynamic Modeling of the Human Knee to Include Tibio-Femoral and Patello-Femoral Joints," ASME J. Biomech. Eng., **126**(1), pp. 44–53.

[15] DeFrate, L. E., Nha, K. W., Papannagari, R., Moses, J. M., Gill, T. J., and Li, G., 2007, "The Biomechanical Function of the Patellar Tendon During in-Vivo Weight-Bearing Flexion," J. Biomech., **40**(8), pp. 1716–1722.

[16] Yue, B., Varadarajan, K. M., Ai, S., Tang, T., Rubash, H. E., and Li, G., 2011, "Differences of Knee Anthropometry Between Chinese and White Men and Women," J. Arthroplasty, **26**(1), pp. 124–130.

[17] Caruntu, D. I., Hefzy, M. S., Goel, V. K., Goitz, H. T., Dennis, M. J., and Agrawal, V., 2003, "Modeling the Knee Joint in Deep Flexion: Thigh and Calf Contact," Proceedings of 2003 Summer Bioengineering Conference, Key Biscayne, Florida, June 25–29, pp. 459–460.

[18] Granados, E., 2015, "Two-Dimensional Dynamics Model of the Lower Limb to Include Viscoelastic Knee Ligaments," MS thesis, The University of Texas Pan-American, Edinburg, TX.

[19] Hill, P. F., Vedi, V., Williams, A., Iwaki, H., Pinskerova, V., and Freeman, M. A., 2000, "Tibiofemoral Movement 2: The Loaded and Unloaded Living Knee Studied by MRI," J. Bone Jt. Surg., **82-B**(8), pp. 1196–1198.

[20] Shelburne, K. B., and Pandy, M. G., 1998, "Determinants of Cruciate-Ligament Loading During Rehabilitation Exercise," Clin. Biomech., **13**(6), pp. 403–413.

[21] Abdel-Rahman, E. M., and Hefzy, M. S., 1998, "Three-Dimensional Dynamic Behavior of the Human Knee Joint Under Impact Loading," Med. Eng. Phys., **20**(4), pp. 276–290.

[22] Most, E., Axe, J., Rubash, H., and Li, G., 2004, "Sensitivity of the Knee Joint Kinematics Calculation to Selection of Flexion Axes," J. Biomech., **37**(11), pp. 1743–1748.

[23] Winter, D. A., 2009, *Biomechanics and Motor Control of Human Movement*, John Wiley & Sons, Hoboken, NJ.

[24] Blajer, W., Dziewiecki, K., and Mazur, Z., 2007, "Multibody Modeling of Human Body for the Inverse Dynamics Analysis of Sagittal Plane Movements," Multibody Syst. Dyn., **18**(2), pp. 217–232.

[25] Niu, W., Feng, T., Jiang, C., Zhang, M., and Khraibi, A. A., 2014, "Peak Vertical Ground Reaction Force During Two-Leg Landing: A Systematic Review and Mathematical Modeling," BioMed Res. Int., **2014**(1), pp. 1–10.
[26] Samozino, P., Morin, J.-B., Hintzy, F., and Belli, A., 2008, "A Simple Method for Measuring Force, Velocity and Power Output During Squat Jump," J. Biomech., **41**(14), pp. 2940–2945.
[27] Cleather, D. J., Goodwin, J. E., and Bull, A. M. J., 2013, "Hip and Knee Joint Loading During Vertical Jumping and Push Jerking," Clin. Biomech., **28**(1), pp. 98–103.
[28] Kernozek, T. W., and Ragan, R. J., 2008, "Estimation of Anterior Cruciate Ligament Tension From Inverse Dynamics Data and Electromyography in Females During Drop Landing," Clin. Biomech., **23**(10), pp. 1279–1286.
[29] Murakami, K., Hamai, S., Okazaki, K., Ikebe, S., Shimoto, T., Hara, D., Mizu-Uchi, H., Higaki, H., and Iwamoto, Y., 2016, "In Vivo Kinematics of Healthy Male Knees During Squat and Golf Swing Using Image-Matching Techniques," Knee, **23**(2), pp. 221–226.